Forces in Mechanics 10 (2023) 100170

Contents lists available at ScienceDirect

Forces in Mechanics

journal homepage: www.sciencedirect.com/journal/forces-in-mechanics

Axial and radial crushing behaviour of thin-walled carbon fiber-reinforced polymer tubes fabricated by the real-time winding angle measurement system

Quanjin Ma [a,b,*], M.R.M. Rejab [*,a,b], Mohammad Azeem [c], M.S. Idris [a], M.F. Rani [d], A.Praveen Kumar [e]

[a] Structural Performance Materials Engineering (SUPERME) Focus Group, Faculty of Mechanical & Automotive Engineering Technology, Universiti Malaysia Pahang, 26600 Pekan, Pahang, Malaysia
[b] School of Mechanical Engineering, Ningxia University, 750021 Yinchuan, China
[c] Department of Mechanical Engineering, Universiti Teknologi PETRONAS, Seri Iskander 32610, Malaysia
[d] Faculty of Engineering, DRB-Hicom University of Automotive Malaysia, 26607 Pekan, Pahang, Malaysia
[e] Department of Mechanical Engineering, Easwari Engineering College, Chennai, India

ARTICLE INFO

Keywords:
Filament winding
Real-time winding angle measurement system
Thin-walled structure
CFRP
Axial and radial loading

ABSTRACT

This paper proposed a real-time winding angle measurement device embedded in the portable 3-axis winding machine, which was used to detect and measure the winding angle during the winding process. The device was completely designed, fabricated, tested, and divided into hardware and software sections. The hardware section was adopted Raspberry Pi 3B+ and Arducam 5MP OV5647 camera modules, and the software section was used the OpenCV software. The experimental test was carried out to validate the measurement data on ±45°, ±60°, and ±75° winding angles, and filament-wound carbon fiber-reinforced polymer tubes were performed the quasi-static radial and axial compression tests. It was found that the real-time measurement data from the system had approximately 0.45±0.02 comparative error value than the targeted winding angle, which was more accurate than traditional measurement data. Moreover, it was shown that peak crushing loading significantly increased with increasing winding angle under radial compression, which had the inverse decreasing trend under axial loading. In addition, the crushing behaviour of thin-walled CFRP tubes was studied.

1. Introduction

Recently, society has drawn growing concerns about environmental sustainability and lightweight transportation. Thin-walled structures made of lightweight composites, e.g., carbon fiber-reinforced polymer (CFRP) and glass fiber-reinforced polymer (GFRP), have been increasingly used as energy-absorbing components [1,2], which is attributed to their higher stiffness-to-weight and reasonable strength. Filament-wound composite structures have been used in various sectors, such as gas and oil piping systems [3], crash boxes [4], and composite pressure vessels (CPVs) due to their high corrosion resistance and good fatigue properties [5]. Filament winding is considered the most suitable automated fabrication method for manufacturing axisymmetric composite structures [6]. It is known that composite pressure vessels are manufactured via filament winding process in the industrial sector. For filament-wound composite structures, various factors significantly affect the structural performance, such as winding angle and pattern [7,8], which mainly depended on the winding capability of the equipment.

To improve the winding capability and quality of filament-wound composite products, many researchers have developed various filament winding machines with multi-axis motions [9,10]. For example, Quanjin et al. investigated the experimental assessment of the 3-axis filament winding machine [11]. It was concluded that the portable 3-axis winding machine provided a 0.83 to 1.13 mm winding circular distance. Andrianov et al. examined the analytical equations for the winding trajectory of the 4-axis winding machine [12]. The preliminary

Abbreviations: ASTM, American Society for Testing and Materials; CFRP, Carbon fiber-reinforced polymer; CFE, Crushing force efficiency; GFRP, Glass fiber-reinforced polymer; CNC, Computer numerical control; CPVs, Composite pressure vessels; EA, Energy absorption; NEMA, National Electrical Manufacturers Association; SEA, Specific energy absorption.

* Corresponding authors.
E-mail addresses: neromaquanjin@gmail.com (Q. Ma), ruzaimi@ump.edu.my (M.R.M. Rejab).

https://doi.org/10.1016/j.finmec.2023.100170
Received 16 November 2022; Received in revised form 29 December 2022; Accepted 15 January 2023
Available online 16 January 2023

trials were shown that the winder lays the fiber straight along the geodesic trajectory. Moreover, Mateen et al. developed a low-cost 2-axis laboratory-size filament winding machine, which achieved a winding angle ranging from 10° to 90° [13]. Furthermore, Abdalla et al. fabricated the 2-axis lathe-type winding machine, which provided 13.6 rpm (rpm) while the speed of the delivery unit varied from 0 rpm to a maximum of 250 rpm [14].

Filament wound composite products have great opportunities in aerospace and automotive engineering [15–17], in which crashworthiness signifies a critical criterion for maintaining structural integrity and safety in sudden collisions. For instance, Sun et al. investigated the oblique lateral crashworthy characteristics of thin-walled circular tubes with aluminum/GFRP/CFRP materials [18]. It was observed that the delamination became less severe with increasing the loading angle due to the drop in crushing loading magnitude. Zhu et al. explored the energy-absorbing mechanisms and structural crashworthiness of laterally crushed thin-walled structures [19]. It was mentioned that the energy-absorbing capacity could be slightly improved by increasing the cell number, proportion of 45° layer, or foam density. Furthermore, Wang et al. manufactured the braided-textile reinforced multi-walled tubular structures as low-cost, lightweight components [20]. It was found that the foam-filling technique and the sandwich structure are both effective methods to improve energy absorption efficiency. In addition, Ma et al. [21] proposed the multi-objective optimization for CFRP/AL hybrid circular tubes, which exhibited better specific energy absorption under three-point bending and axial compression loadings.

In addition, various accessorial equipment or devices [22] have been developed to measure or evaluate filament-wound products, which can improve product quality [23]. For example, Hopmann et al. developed the Infrared-optical system to detect the fiber bandwidth and winding angle, which provided a new method based on an IR inline acquisition system during wet winding [24]. Furthermore, Toptaş developed the damage detection of carbon fiber using an electrical resistance method [25]. It was demonstrated that the electrical conductive property of carbon fiber could effectively evaluate the damage during the winding process. Filament wound composite products are known to be widely measured by the digital microscope, angle protector, or computerized algorithm. Although several works have been reported to develop the accessorial components on the existing winding machine, limited works have paid attention to the non-contact measurement method that measures the winding angle of filament-wound composite structures. Here, there is an urgent requirement and particular importance to detecting and measuring the winding angle during the winding process.

This paper aims to develop a real-time winding angle measurement system that integrates with the 3-axis winding machine. The winding angle detection and measurement results were analyzed and visualized on the captured images. Moreover, the effect of winding angle on crashworthiness characteristics of thin-walled CFRP tubes was investigated under radial and axial compression. Several parameters are calculated and analyzed under two loading directions: compressive strength and modulus, energy absorption, and specific energy absorption. In addition, the radial and axial crushing behavior of CFRP tubes were analyzed.

2. Materials and methods

2.1. Design procedure of the real-time winding angle measurement system

The V-shape slot aluminum extrusion, V-shape slot rollers, a timing belt and pulley, a toothed idler, several 3D printed holders, and the National Electrical Manufacturers Association (NEMA) 17-stepper motor were assembled. The motorized slider can have linear movement of the camera to inspect the winding angle along the mandrel. A V-shape slot aluminum extrusion profile was acted as the slider track, which was fixed to the 3-axis winding machine with L-shape brackets. The slider track was controlled and activated, which was synchronized with the winding process. The control box was contained the Raspberry Pi 3B+ module, and the camera was placed on the slider position. For the 3-axis winding machine, the hardware section was adopted the Arduino UNO microcontroller and computer numerical control (CNC) V1 shield module [26]. The Universal G-code Sender software was used in the software section, which sent the programmed G-codes to perform the winding process [27]. Fig. 1 illustrates the electrical circuit diagram of Arduino UNO and Raspberry Pi 3B+ microcontrollers. The Arduino UNO was the main channel for transferring signals, which started by supplying power to the stepper motor to initiate slider movement. The travelled distance by slider was performed in the CNC shield module, which transferred the signal for the winding angle acquisition through Raspberry and the camera [28].

2.2. Real-time winding angle measurement procedure

The real-time winding angle system was developed to measure the winding angle during the dry or wet winding process. Three winding angles were programmed using the G-codes, and the dry winding process was performed in the laboratory scale 3-axis winding machine [29]. The proposed system was integrated with the available 3-axis winding machine. The hardware section was adopted Raspberry Pi 3B+ and Arducam 5MP OV5647 camera module. The software section of the system was used OpenCV software, which was programmed through Python language. Fig. 2 illustrates the real-time winding angle measurement procedure. The real-time winding angle measurement system detected and measured the winding angle by two color-detected lines. The corresponding measurement data was collected and shown in the dialog box. The green color line was set as the targeted winding angle (±45°, ±60°, and ±75°). The red color line was defined as the winding angle exceeding 1°, which was deleted from the collected data, as illustrated in Fig. 2(a). The detection mechanism was based on the definition of winding angle, which was the angle between the fiber tow and axis line, as shown in Fig. 2(b).

2.3. Fabrication of filament wound CFRP tube

The carbon fiber tow was used PYROFIL™ TR30S 3 K, which provided by Mitsubishi Chemical Carbon Fiber and Composites, Inc. The resin system was used the EpoxAmite™ 100 epoxy laminating system with 102 Medium Hardener by Smooth-On, Inc., which was mixed as the recommended weight ratio of 100:29. Filament-wound CFRP tubes were manufactured by the laboratory scale 3-axis filament winding machine integrated with the real-time winding angle measurement system. Laminates were accomplished with the programmed G-codes, in which the main parameters are controlled: winding trajectory, angle, and pattern [6]. Specifications of TR30S 3 K carbon fiber and EpoxAmite™ 100 epoxy resin are shown in Table 1.

This study used the aluminum mandrel (outer diameter: 38 mm) to manufacture the CFRP tubes. After wet winding, the initial filament wound composite tube was fully cured for 24 h with 10 rpm mandrel rotation movement [30]. The composite tube was later removed from the mandrel. The tube was cut into 55 mm length and polished using Forcipol grinder-polisher equipment. The geometric dimension of CFRP tube, i.e., thickness, diameter-thickness ratio (d/t), length-diameter ratio (l/d), inner diameter-outer diameter (d_i/d_o), and winding angle of laminates are summarized in Table 2. Fig. 3 illustrates the thin-walled CFRP tubes in this study.

2.4. Quasi-static compression test

Filament wound CFRP tubes were tested under quasi-static axial and radial compression. Two tests have been carried out in the Universal Test Machine Instron 3369 model with a 50 kN load capability. There are at least three specimens to validate the experimental results. An axial compression test was conducted with a speed rate of 2 mm/min, which

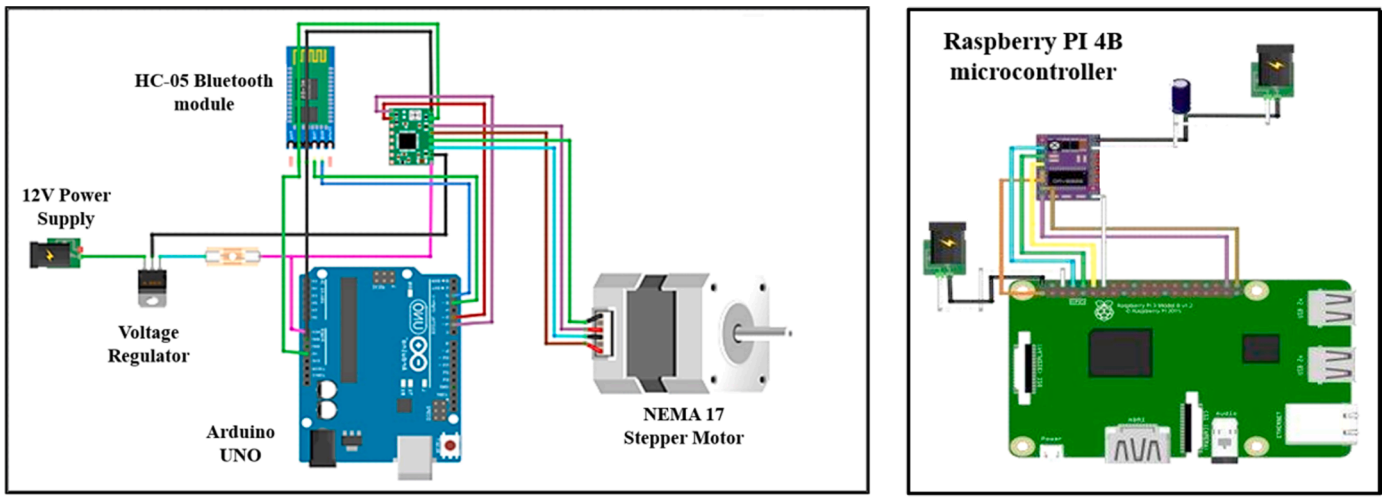

Fig. 1. Electrical circuit diagram of Arduino UNO and Raspberry Pi 3+ microcontrollers.

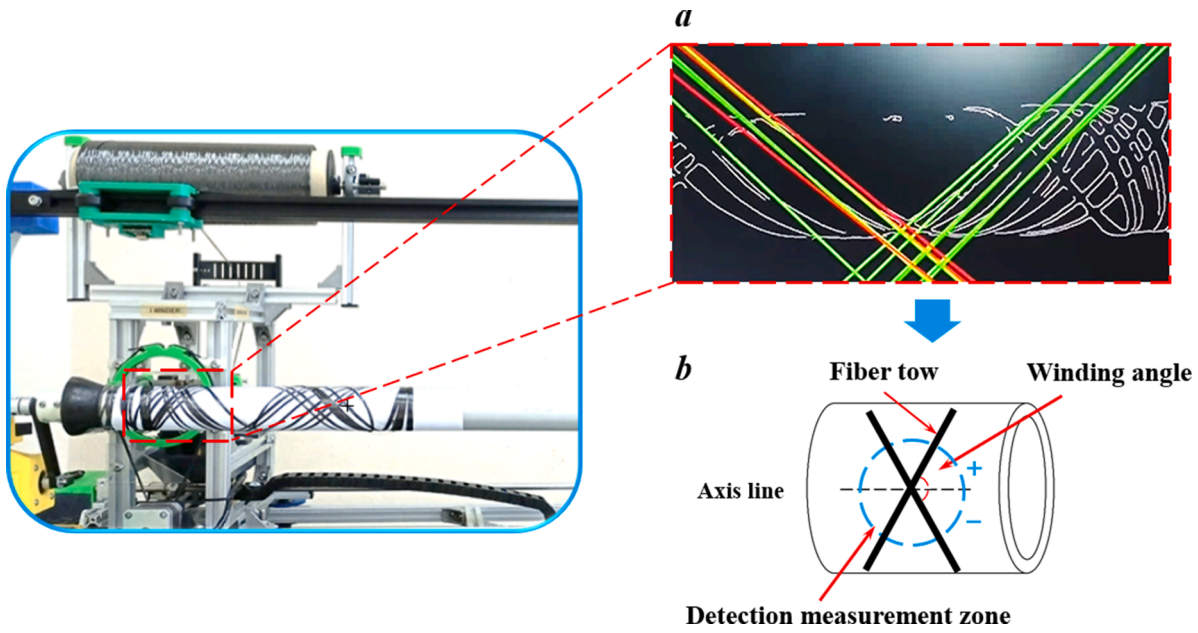

Fig. 2. Real-time winding angle measurement procedure: (a) detection and measurement of visual data; (b) measurement mechanism.

Table 1
Specifications of TR30S 3 K carbon fiber and EpoxAmite™ 100 epoxy laminating system.

Specification	TR30S 3K	Specification	EpoxAmite™ 100 epoxy resin /102 Medium Hardener
Type	TR 30S 3L	Mix ratio by volume	3:1
Number of filaments	3000	Mix ratio by weight	100:29
Filament diameter (μm)	7	Mixed viscosity	0.65
Yield (mg/m)	200	Pot life (hour)	0.37
Tensile strength (MPa)	4120	Curing time (hour)	10–15
Tensile modulus (GPa)	234	Specific gravity (kg/l)	1.11
Elongation (%)	1.80	Compressive strength (MPa)	75
Density (g/cm^3)	1.79	Tensile elongation	3.15

Table 2
Summary of thin-walled filament wound CFRP tubes.

Labels	Winding angle (°)	Number of plies	Thickness (mm)	Mass (g)	l/d	d/t	d_i/d_o
CFRP45	$[\pm 45°]_2$	2	1.2	9.5	1.3	34.6	0.9
CFRP60	$[\pm 60°]_2$	2	1.2	9.4	1.3	34.6	0.9
CFRP75	$[\pm 75°]_2$	2	1.2	9.4	1.3	34.6	0.9

was followed by the ASTM D5449 [31], as shown in Fig. 5(a). The axial compression test studies the crushing behavior of filament wound CFRP tubes. Furthermore, a radial compression test was performed at a speed rate of 2 mm/min following the ASTM D2412–11 [32], which pays attention to the loading characteristics of composite tubes under two parallel platens, as shown in Fig. 5(b). The load versus displacement curves were obtained by Bluehill Universal software, and the failure behavior of specimens was recorded during the quasi-static axial and radial compression tests. Fig. 4 illustrates the experimental setup of quasi-static axial and radial compression tests.

Fig. 3. Thin-walled filament wound CFRP tubes fabricated by laboratory scale 3-axis winding machine.

In addition, several parameters were adopted to quantify the crashworthiness characteristics [31,33,34], such as mean crushing loading (F_{mean}), peak crushing loading (F_{peak}), compressive strength (σ), compressive modulus (E), energy absorption (EA), specific energy absorption (SEA), crushing force efficiency (CFE).

The peak crushing loading (F_{peak}) is obtained from the load versus displacement. The mean crushing loading is calculated, and d is the crushing distance.

$$F_{mean} = \frac{EA}{d} \tag{1}$$

Compressive strength (σ) is calculated as,

$$\sigma = \frac{F}{A} \tag{2}$$

Where F is applied loading, A is the cross-sectional area. For axial loading, A_a is 152.22 mm^2. For radial loading, A_r is used in the planar area as 2.28×10^3 mm^2.

Compressive modulus (E) is the slope of the stress versus strain curve and is calculated as follows:

$$E = \frac{\Delta\sigma}{\Delta\varepsilon} \tag{3}$$

Energy absorption (EA) is defined as the area below the load versus displacement curve, which is calculated mathematically as follows:

$$EA = \int_0^d F(x)dx \tag{4}$$

Specific energy absorption (SEA) is used to indicate the energy absorption capability, which is defined as the amount of energy absorbed per unit mass.

$$SEA = \frac{EA}{m} \tag{5}$$

Where m is the mass of the filament wound CFRP tube.

Crushing force efficiency (CFE) is used to measure the uniformity of crushing loading and calculated as,

$$CFE = \frac{F_{mean}}{F_{peak}} \tag{6}$$

2.5. Burn-out test

The burn-out test was performed using a Nabertherm furnace, which put the specimen at 500 °C for 1 h according to ASTM D2584–94 [35]. Specimen weight was measured before and after the test, which was used to calculate fiber mass fraction [36]. The experimental setup of the burn-out test is illustrated in Fig. 5. It was better to use mass fraction volume to calculate the mass fraction distribution due to its circular shape.

3. Results and discussion

3.1. The real-time winding angle measurement system

Fig. 6 presents the laboratory scale 3-axis winding machine integrated with the real-time winding angle measurement system. The real-

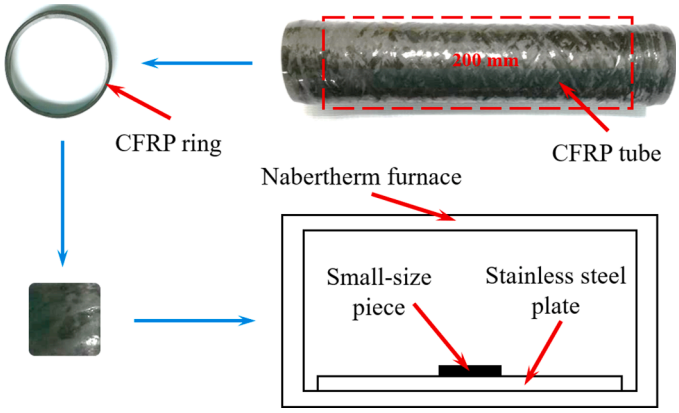

Fig. 5. Burn-out test of the small-size piece from a thin-walled filament wound CFRP tube.

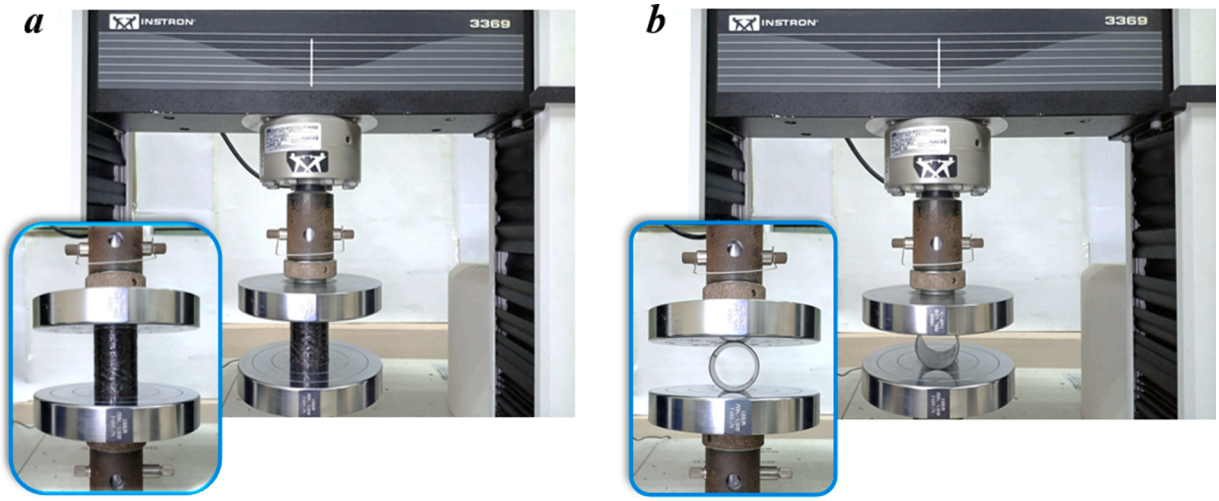

Fig. 4. Experimental setup: (a) quasi-static axial compression test; (b) quasi-static radial compression test.

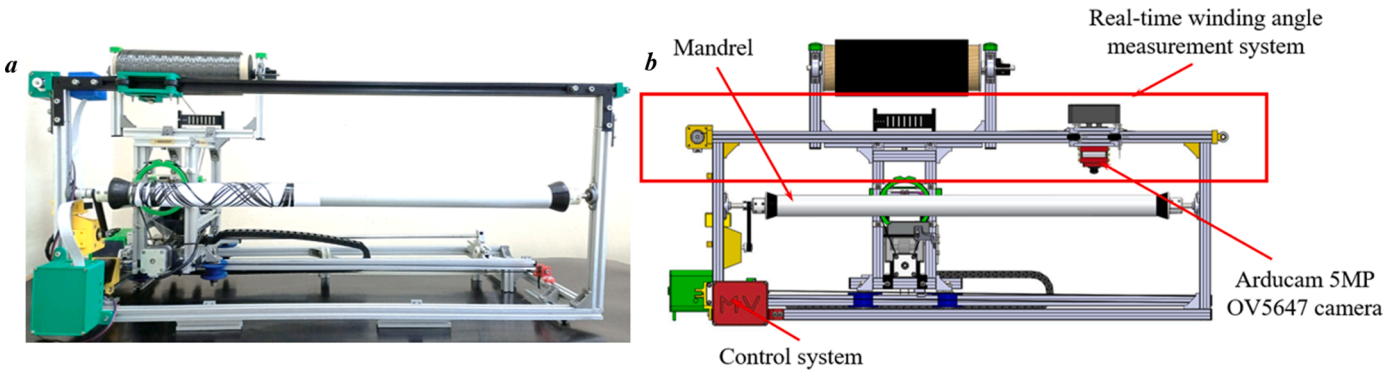

Fig. 6. Laboratory scale 3-axis winding machine integrated with the real-time winding angle measurement system: (a) realized machine prototype; (b) 3D Solidworks machine design prototype.

time winding angle measurement device consists of three parts: the machine vision slider, the machine vision holder, and the control system. The real-time winding angle measurement system mainly consists of a Raspberry Pi 3B+ and an Arducam 5MP OV5647 camera, which provides an open-source system with inexpensive costs. The slider can adjust the distance between the camera and the mandrel, which provides a high-resolution captured image. An experimental test of the real-time measurement system was detected and measured the single fiber tow during the dry winding process.

3.2. Results of real-time winding angle measurement data

Arducam OV5647 5MP camera, OpenCV framework, and the Raspberry Pi 3B+ were used to measure the real-time winding angle. The system was processed and measured using the OpenCV framework, which was used to confirm the detected angle inside or outside of the winding angle range. Fig. 7 presents the results of winding angle data in the winding process and visualization interface image. Two color lines were detected to measure the winding angle. The green line was set as measurement data on the winding angle. The red line was out of the targeted winding angle with 1° tolerance, and measurement data was deleted.

To validate the real-time winding angle measurement data, three winding angles (±45°, ±60°, and ±75°) were performed on the dry winding process. The real-time measurement system was detected when the single trajectory was completed. Three winding angles were wound in the mandrel with 220 mm length, which showed the targeted winding angle detection capability. Fig. 8 exhibits the visual images in the real-time winding angle measurement system. It was found that each winding angle was fully detected and measured with green and red lines. The detection procedure was overperformed with multiple lines, and measurement data were obtained on each captured line. Moreover, it was found that the winding angle was quickly detected and measured in the mandrel center. It might be explained by the circular shape of the mandrel, which provided the different perpendicular distance to the camera.

The 3 K fiber tow was 3 mm in width, which was used to measure the contiguous tow distance with three winding angles under the dry winding process. The contiguous tow distance has defined the distance between the two contiguous tow paths, which was used to evaluate the winding accuracy and performance on different winding angles. The contiguous tow distance of each winding angle was measured six times to provide accurate results. Fig. 9 presents the definition of contiguous tow distance and the results of the contiguous tow distance on three winding angles. It was obtained that the contiguous tow distance was 1.05 mm for ±45° winding angle, 1.00 mm for ±60° winding angle, and 0.83 mm for ±75° winding angle. It was found that with the winding angle increased, the contiguous fiber tow distance decreased [11]. The laboratory scale 3-axis winding machine integrated with the real-time winding angle measurement system can provide 0.83 to 1.05 mm contiguous tow distance.

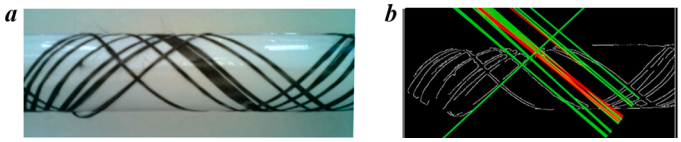

Fig. 7. Results of winding angle data: (a) captured image in the mandrel; (b) visualization interface image in the real-time winding angle measurement system.

The traditional method was used the digital microscope to measure the winding angle on filament wound CFRP tubes. The proposed system adopted real-time measurement system data to measure the winding angle during the winding process. Here, ten measurement data of each winding angle on two methods were collected and analyzed. Fig. 10 illustrates the results of comparative error value about winding angle on traditional and real-time measurement system data. It was shown that the real-time measurement data from the system provided a 0.45±0.02 comparative error value than the targeted winding angle. Moreover, it was observed that the real-time measurement data from the system was much more accurate in winding angle measurement results than the traditional measurement method. In addition, it was highlighted that the winding angle measurement accuracy from the system provided stable data on ±45°, ±60°, and ±75° winding angles.

In addition, the advantages and disadvantages of the two methods were discussed and compared. The traditional method used the protractor or digital microscope equipment to assess the winding angle, which was measured on the surface of filament-wound composite products. There are several disadvantages or inconveniences to the traditional method, such as labor costs, examination area (usually only outside surface), high indirect measurement error, and interlayer examination issues. The real-time measurement method was non-contact, according to the real-time visual image. There are many advantages to the real-time measurement method, such as cost saving, each layer examination, automatic measurement, high measurement efficiency, range, etc. Some potential issues or disadvantages of the real-time measurement method are mentioned according to the authors' experience. The system may not capture the visual image to provide the measurement data for high mandrel rotation speed. For the wet winding process, the resin and the surface condition of the mandrel may reduce the measurement accuracy of this system.

3.3. Result of burn-out test on CFRP tubes

Burn-out test results of CFRP tubes were obtained, and average fiber weight fraction results were used to evaluate the overall quality of the composite tube. It was found that the average fiber mass fraction was

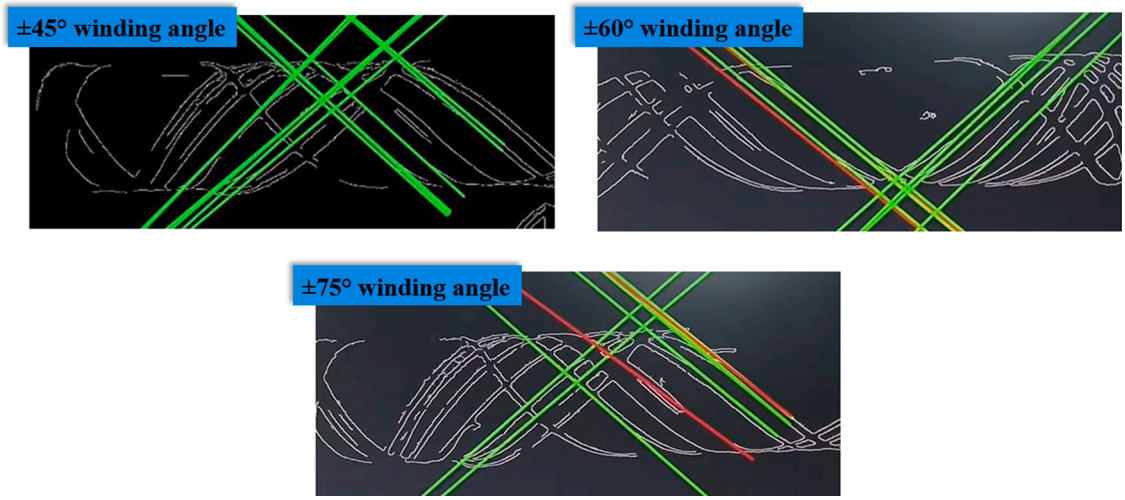

Fig. 8. Results of visual images in the real-time winding angle measurement system.

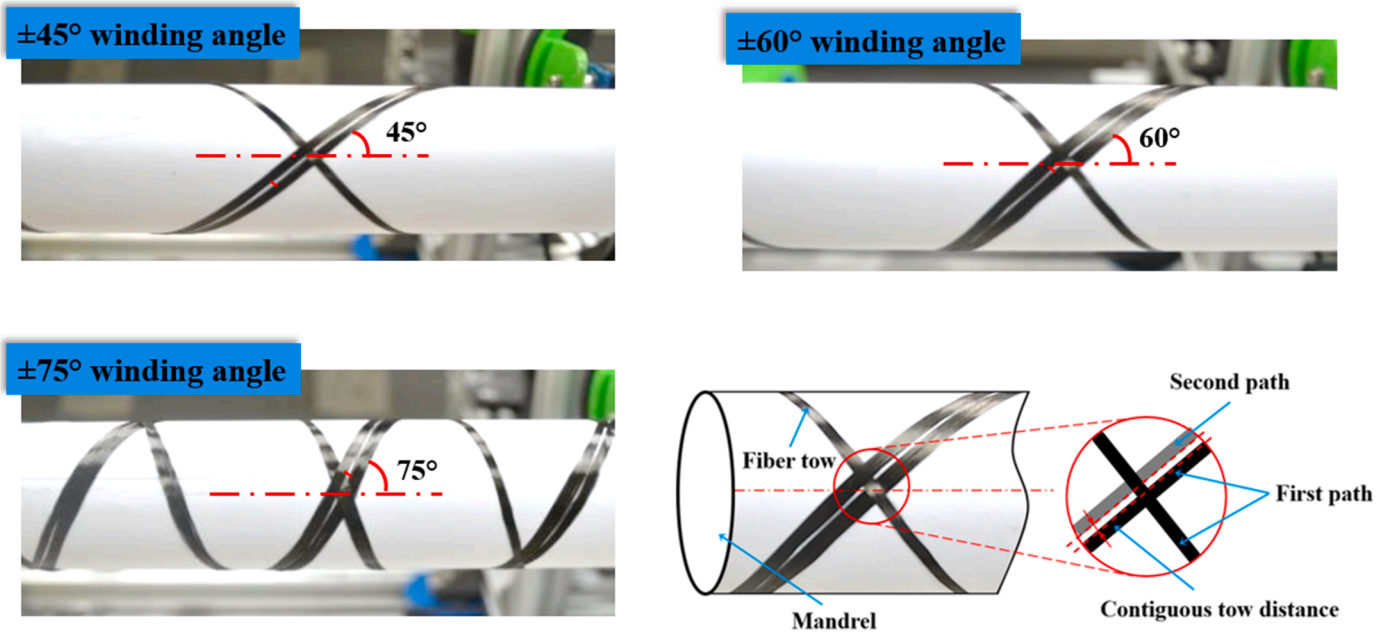

Fig. 9. Schematic diagram and measurement procedure of the contiguous tow distance on ±45°, ±60°, and ±75 winding angles under the winding process.

39.93%± 0.03 for ±45° winding angle, 40.63%± 0.02 for ±60° winding angle, and 46.77% ± 0.01 for ±75° winding angle. The fiber mass fraction value of composite tubes ranged from 39.93% to 46.77%.

3.4. Result of CFRP tube under radial and axial loading

Load versus displacement curves of CFRP tubes with ±45°, ±60°, and ±75° winding angles under radial and axial compression were plotted in Fig. 11. It was found that peak crushing loading increased under radial compression with increasing winding angle, as shown in Fig. 11(a). It was attributed that the closer the winding angle to the loading direction, the higher the peak crushing load occurred [37,38]. For the [±60°] and [±75°] specimens, the loading reached the peak crushing load with a similar deflection of around 13 mm, which provided a more linear-elastic behavior. Then, two minor peaks were observed due to the delamination [18,38]. Meanwhile, the high non-linearity was plotted, which was associated with the lateral deflection and bending of the composite tube.

Fig. 11(b) plots composite tube load versus displacement curves under axial compression. It was obtained that the [±45°] specimen had the maximum peak crushing loading. The closer the winding angle is to the loading direction, the higher the maximum peak load achieved [37]. It was observed that unstable local buckling deformation in the thin-walled tube wall and some transverse cracks, fiber fracture outwards, and fragments were initiated and propagated under the plastic deformation stage. It was highlighted that the initial cracks paralleled the winding angle following the axial loading direction, which agreed with other similar findings [7,37,38].

Furthermore, nominal stress versus nominal strain curves of CFRP tubes stress versus strain curves of CFRP tubes under radial and axial compression are shown in Fig. 12. For radial compression, the [±75°] specimen obtained the maximum nominal stress value of 0.31 MPa, which was 1.72 times compared to the [±45°] specimen with 0.18 MPa. For axial compression, the [±45°] specimen provided the maximum nominal stress value of 69.83 MPa, which was 1.25 times that of to [±75°] specimen with 55.74 MPa. The result revealed the opposite

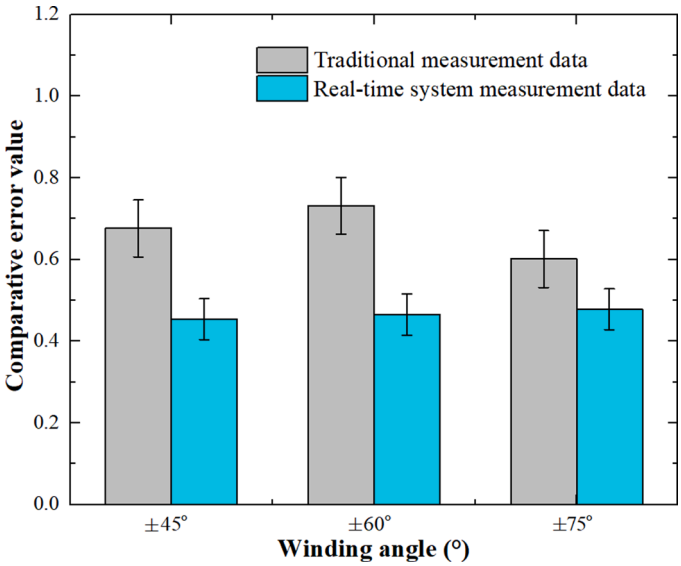

Fig. 10. Results of comparative error value about winding angle on traditional and real-time measurement system data.

maximum and minimum nominal stress on ±45° and ±75° winding angles, which was attributed to the loading direction (radial and axial directions).

Damage behavior of the CFRP tube under radial and axial compression loading is illustrated in Fig. 13, which is analyzed in the crushing failure mode under two compression directions. Fig. 13(a) shows the photographs of the CFRP tube under axial compression. The unstable buckling deformation and a few cracks were observed in the thin wall. Then, some cracks and outwards fronds were initiated and propagated, which was mainly due to fiber fracture, matrix damage, transverse shearing, and friction between the tubular wall and the crosshead. Fig. 13(b) records the photographs of the CFRP tube under radial compression. Delamination was mainly observed on the thin-walled CFRP tube under radial loading. The CFRP specimens with three winding angles exhibited longitudinal fracture lines, in which the first two fracture lines originated around the two boundary contact lines between the wall and rigid platens. Interestingly, it was found that the fracture line was located at a 90° phase angle, which agreed with other research findings [38,18].

3.5. Effect of winding angle on filament wound CFRP tube

Several important parameters are studied and analyzed under radial and axial compression to investigate the effect of winding angle on filament wound CFRP tube. Fig. 14 plots the F_{mean} and F_{peak} of CFRP tubes with three winding angles. For radial compression, it was shown that with increasing the winding angle, F_{mean} and F_{peak} exhibited an increasing trend, as illustrated in Fig. 14(a). The maximum F_{mean} and F_{peak} appeared at [±75°] specimen, which was 0.35±0.03 kN and 0.69 ±0.05 kN. F_{mean} and F_{peak} exhibited a decreasing trend for axial compression with increased winding angles, as shown in Fig. 14(b). Therefore, the maximum F_{mean} and F_{peak} were obtained at ±75° winding angle, which was 4.41±0.48 kN and 10.63±0.51 kN.

Moreover, the compressive strength and modulus of CFRP tubes with three winding angles are depicted in Fig. 15. For radial compression, it was revealed that increasing the winding angle, compressive strength, and modulus had an increasing trend. The maximum compressive strength and modulus were 0.31±0.02 MPa and 1.09±0.05 MPa. For axial compression, the decreasing trend was observed as increasing the winding angle, as shown in Fig. 15(b). Here, the maximum compressive strength and modulus were 69.83±3.23 MPa and 1745.75±150.17 MPa at a ±45° winding angle, which was 1.25 times higher than the minimum compressive strength and modulus (55.77±5.46 MPa and 1394.25 ±50.32 MPa) at ±75° winding angle.

Here, it is essential to study the effect of winding angle on *EA* and *SEA* under radial and axial compression. Fig. 16 illustrates the *EA* and *SEA* of CFRP tubes with three winding angles. For radial compression, the maximum *EA* and *SEA* were 12.51 J and 1.32 kJ/kg at ±75° winding angle, which improved 1.37 times than the above two parameters at ±45° winding angle. For axial compression, it was shown a decreasing trend on *EA* and *SEA* from ±45° to ±75° winding angle. It was obtained that the maximum *EA* and *SEA* were 176.65 J and 18.58 kJ/kg at ±45° winding angle. Fig. 17 presents the *CFE* of CFRP tubes with three winding angles. Interestingly, it was shown that as increasing the winding angle, the *CFE* decreased on radial and axial loadings [38]. Therefore, the maximum *CFE* were 0.62 and 0.41 on radial and axial compression at ±45° winding angle. It was shown that the thin-walled CFRP tube could provide much better energy absorption under axial compression direction than in radial compression direction. It is worth noting that the winding angle of filament wound composite tube is

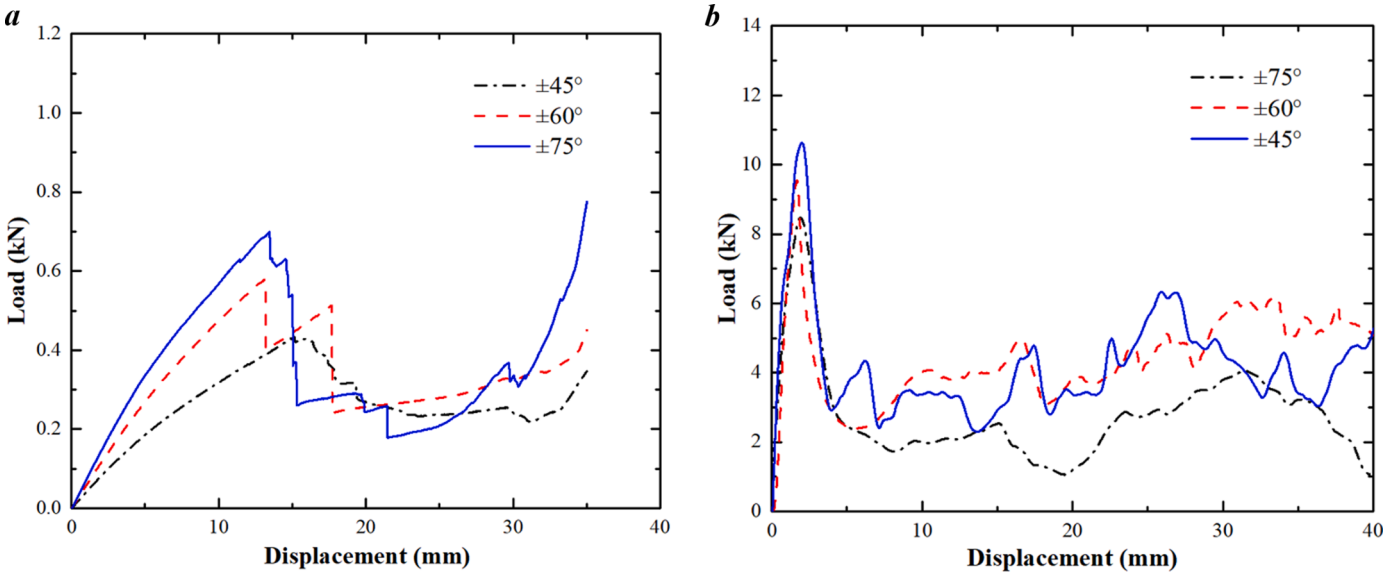

Fig. 11. Load versus displacement curves of CFRP tubes with ±45°, ±60°, and ±75° winding angles: (a) radial compression; (b) axial compression.

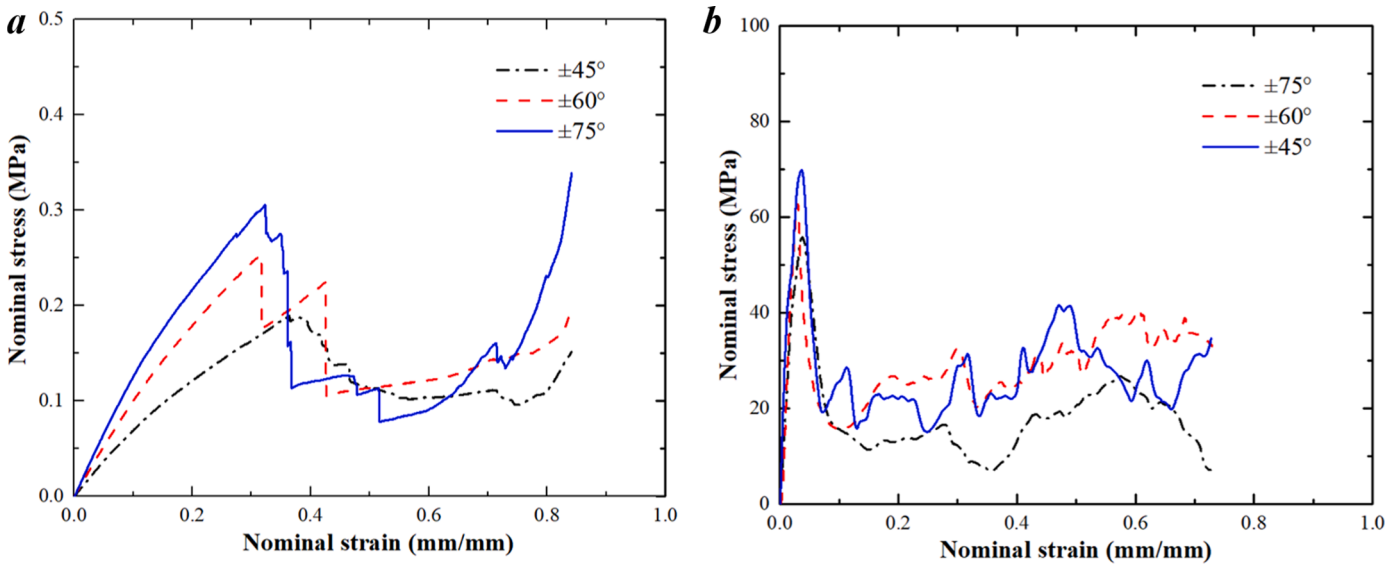

Fig. 12. Nominal stress versus nominal strain curves of CFRP tubes with ±45°, ±60°, and ±75° winding angles: (a) radial compression; (b) axial compression.

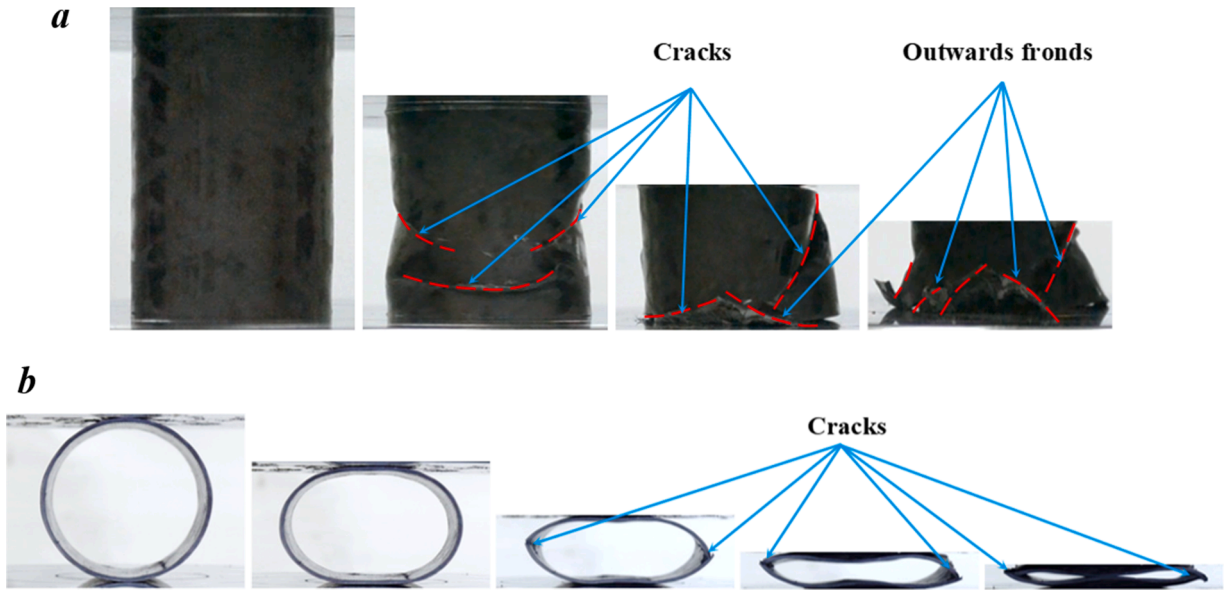

Fig. 13. Crushing behavior of CFRP tubes: (a) axial compression; (b) radial compression.

significantly considered.

4. Conclusion

The real-time winding angle measurement system was developed, tested, and integrated with the laboratory scale 3-axis winding machine. The experimental study of thin-walled CFRP tubes was conducted under radial and axial compression, which investigated the effect of winding angle. Within the limitation of this study, the following conclusions can be drawn:

The real-time winding angle measurement system embedded with the 3-axis winding machine was successfully developed, assembled, and tested. Raspberry Pi 3B+ and Arducam 5MP OV5647 camera adopted the winding angle measurement system, which provided open-source software. Experimental tests of the real-time measurement system were detected, and the contiguous tow distance was measured with three winding angles under the dry winding process.

It was shown that the real-time measurement data from the system provided a 0.45±0.02 comparative error value than the targeted winding angle. It was observed that the real-time measurement data from the system was much more accurate in winding angle measurement results than the traditional measurement method.

For the burn-out test of the CFRP tube, the fiber mass fraction value of the CFRP tube ranged from 39.93% to 46.77%.

For the radial and axial compression test of CFRP, it was found that with increasing winding angle, peak crushing loading increased under radial compression. It was highlighted that the initial cracks paralleled the winding angle following the axial loading direction.

For the effect of winding angle on filament wound CFRP tube, it was shown that with increasing the winding angle, F_{mean} and F_{peak} exhibited the increasing trend under radial compression. For radial compression, the maximum *EA* and *SEA* were 12.51 J and 1.32 kJ/kg at ±75° winding angle, which improved 1.37 times than the above two parameters at ±45° winding angle.

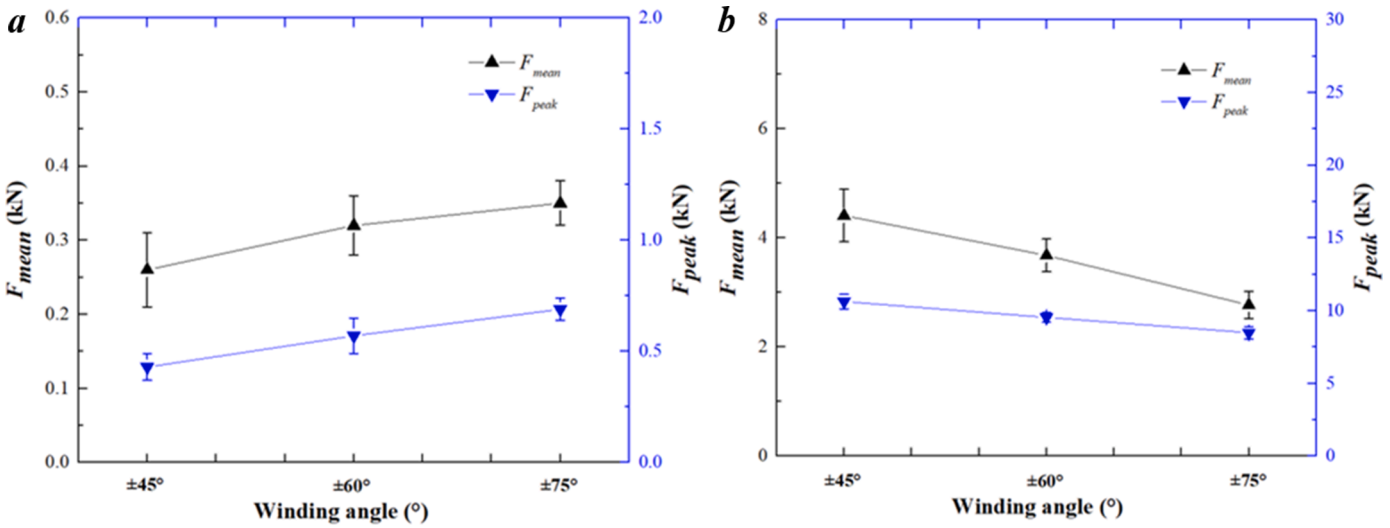

Fig. 14. F_{mean} and F_{peak} of CFRP tubes with ±45°, ±60°, and ±75° winding angles: (a) radial compression; (b) axial compression.

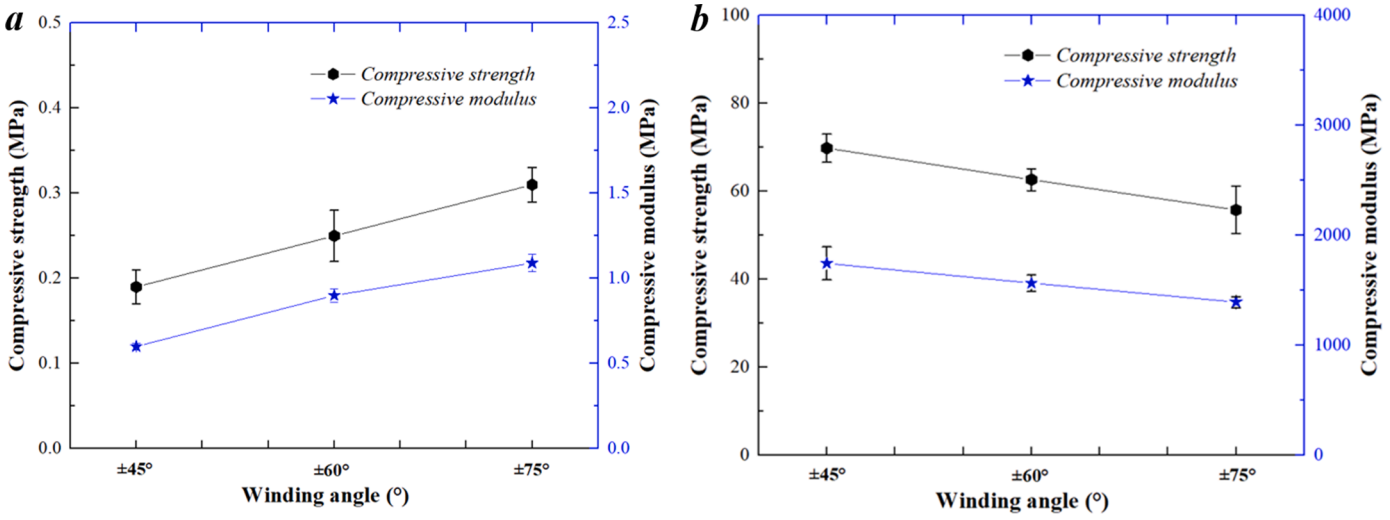

Fig. 15. Compressive strength and modulus of CFRP tubes with ±45°, ±60°, and ±75° winding angles: (a) radial compression; (b) axial compression.

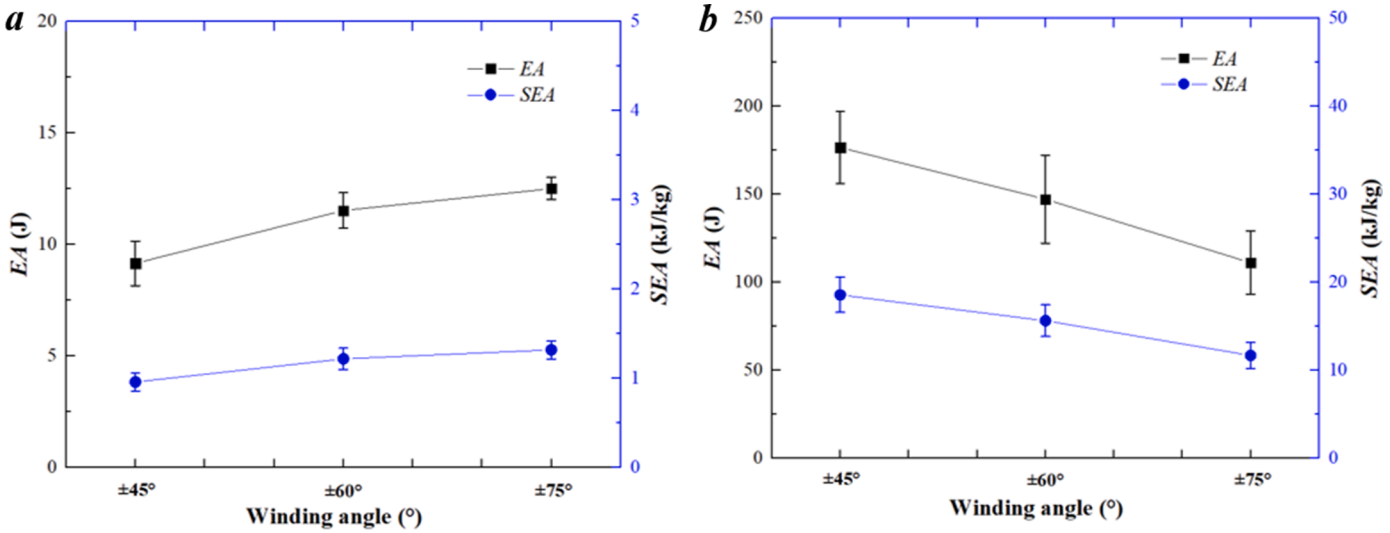

Fig. 16. *EA* and *SEA* of CFRP tubes with ±45°, ±60°, and ±75° winding angles: (a) radial compression; (b) axial compression.

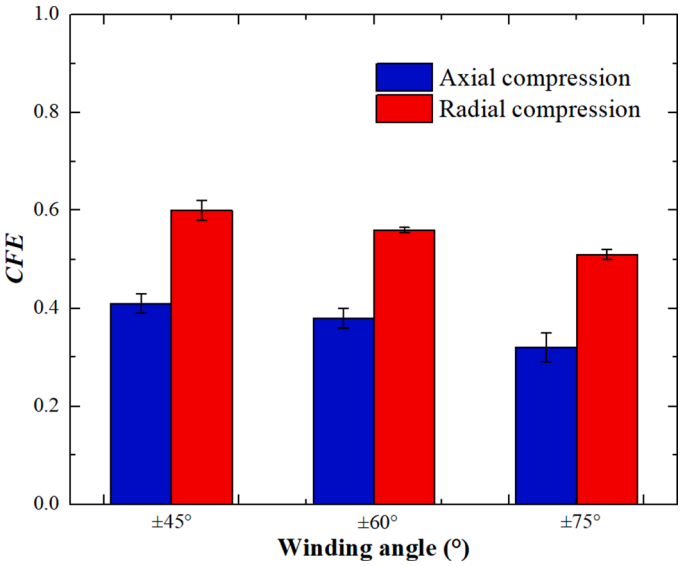

Fig. 17. *CFE* of CFRP tubes with ±45°, ±60°, and ±75° winding angles under radial and axial compression loading tests.

Declaration of Competing Interest

The author(s) declared no potential conflicts of interest with respect to the research, authorship, and/or publication of this article.

Data availability

The authors are unable or have chosen not to specify which data has been used.

Acknowledgement

The authors would like to acknowledge the Faculty of Mechanical & Automotive Engineering Technology, Universiti Malaysia Pahang for funding this research: RDU1901126. The *Structural Performance Materials Engineering (SUPREME) Focus Group* strongly supports this research work.

References

[1] M. Quanjin, M. Salim, M. Rejab, O.-.E. Bernhardi, A.Y. Nasution, Quasi-static crushing response of square hybrid carbon/aramid tube for automotive crash box application, Mater. Today: Proc. 27 (2020) 683–690.
[2] Q. Ma, M. Rejab, S. Kang, M. Idris, M. Zin, The energy-absorbing characteristics of single spherical-roof contoured-core (SRCC) cell with composite materials, Int. J. Autom. Mech. Eng. 17 (4) (2020), 8265–8273-8265–8273.
[3] D.S. Gemi, Ö.S. Şahin, L. Gemi, Experimental investigation of the effect of diameter upon low velocity impact response of glass fiber reinforced composite pipes, Compos. Struct. 275 (2021), 114428.
[4] Q. Ma, Y. Zha, B. Dong, X. Gan, Structure design and multiobjective optimization of CFRP/aluminum hybrid crash box, Polym. Compos. 41 (10) (2020) 4202–4220.
[5] M. Azeem, et al., Application of filament winding technology in composite pressure vessels and challenges: a review, J. Energy Storage 49 (2022), 103468.
[6] M. Quanjin, M. Rejab, J. Kaige, M. Idris, M. Harith, Filament winding technique, experiment and simulation analysis on tubular structure, IOP Confe. Ser. Mater. Sci. Eng. 342 (1) (2018), 012029. IOP Publishing.
[7] P. Stabla, M. Lubecki, M. Smolnicki, The effect of mosaic pattern and winding angle on radially compressed filament-wound CFRP composite tubes, Compos. Struct. 292 (2022), 115644.
[8] M. Quanjin, M. Rejab, M. Idris, B. Zhang, N.M. Kumar, Filament winding technique: SWOT analysis and applied favorable factors, SCIREA J. Mech.Eng. 3 (1) (2019) 1–25.
[9] I. Koustas, T. Papingiotis, G.-.C. Vosniakos, A. Dine, On the development of a filament winding robotic system, Procedia Manuf. 17 (2018) 919–926.
[10] M. Quanjin, M. Rejab, M. Idris, N.M. Kumar, M. Merzuki, Robotic filament winding technique (RFWT) in industrial application: a review of state of the art and future perspectives, Int. Res. J. Eng. Technol. 5 (12) (2018) 1668–1676.
[11] M. Quanjin, M. Rejab, N.M. Kumar, M. Idris, Experimental assessment of the 3-axis filament winding machine performance, Results Eng. 2 (2019), 100017.
[12] A. Andrianov, E.K. Tomita, C.A.G. Veras, B. Telles, A low-cost filament winding technology for university laboratories and startups, Polymers 14 (5) (2022) 1066.
[13] M. Mateen, D.R. Shankar, M.M. Hussain, Design and development of low cost two axis filament winding machine, J. Adv. Manuf. Technol. (JAMT) 12 (1) (2018) 117–126.
[14] F. Abdalla, et al., Design and fabrication of low cost filament winding machine, Mater. Des. 28 (1) (2007) 234–239.
[15] Q. Ma, M. Rejab, J. Siregar, Z. Guan, A review of the recent trends on core structures and impact response of sandwich panels, J. Compos. Mater. 55 (18) (2021) 2513–2555.
[16] C. Bai, Q. Ma, X. Gan, T. Zhou, Theoretical prediction model of mean crushing force of CFRP-Al hybrid circular tubes under axial compression, Polym. Compos. 42 (10) (2021) 5035–5050.
[17] Q. Ma, et al., Fabrication of the carbon fiber reinforced plastic (CFRP) cone tube through the laboratory-scale 3-axis winding machine, Mater. Today: Proc. 46 (2021) 1645–1651.
[18] G. Sun, X. Guo, S. Li, D. Ruan, Q. Li, Comparative study on aluminum/GFRP/CFRP tubes for oblique lateral crushing, Thin Walled Struct. 152 (2020), 106420.
[19] G. Zhu, Z. Zhao, P. Hu, G. Luo, X. Zhao, Q. Yu, On energy-absorbing mechanisms and structural crashworthiness of laterally crushed thin-walled structures filled with aluminum foam and CFRP skeleton, Thin Walled Struct. 160 (2021), 107390.
[20] W. Wang, H. Wang, P. Wang, J. Zhou, H. Fan, Manufacture of braided-textile reinforced multi-walled tubular structures and axial compression behaviors, Compos. Commun. 32 (2022), 101160.
[21] Q. Ma, et al., Multi-objective optimization for energy absorption of carbon fiber-reinforced plastic/aluminum hybrid circular tube under both transverse and axial loading, J. Mater. Eng. Perform. 29 (9) (2020) 5609–5624.
[22] M. Quanjin, M. Rejab, M. Idris, B. Zhang, M. Merzuki, N.M. Kumar, Wireless technology applied in 3-axis filament winding machine control system using MIT app inventor, IOP Conf. Ser.: Mater. Sci. Eng. 469 (1) (2019), 012030. IOP Publishing.
[23] M. Quanjin, M. Merzuki, M. Rejab, M. Noh, Compressive behaviour of aluminium rectangular hollow tube using Digital Image Correlation (DIC) method, IOP Conf. Ser.: Mater. Sci. Eng. 863 (1) (2020), 012038. IOP Publishing.
[24] C. Hopmann, N. Magura, N. Rozo Lopez, D. Schneider, K. Fischer, Detection and evaluation of the fibers' deposition parameters during wet filament winding, Polym. Eng. Sci. 61 (5) (2021) 1353–1367.
[25] E. Toptaş, N. Akkuş, Damage detection of carbon fibers in filament winding machines using an electrical resistance method, Int. J. Adv. Manuf. Technol. 93 (1) (2017) 671–679.
[26] Q. Ma, M. Rejab, M. Idris, Dataset of the lab-scale 3-axis winding machine integrated with the portable real-time winding angle measurement system, Data Brief. 45 (2022), 108731.
[27] M. Quanjin, M. Rejab, M. Idris, B. Bachtiar, J. Siregar, M. Harith, Design and optimize of 3-axis filament winding machine, IOP Conf. Ser.: Mater. Sci. Eng. 257 (1) (2017), 012039. IOP Publishing.
[28] Q. Ma, et al., Development of the real-time winding angle measurement device for the laboratory-scale 3-axis winding machine, Mater. Today: Proc. (2022).
[29] M. Quanjin, et al., Design of portable 3-axis filament winding machine with inexpensive control system, J. Mech. Eng. Sci. 12 (1) (2018) 3479–3493.
[30] M. Quanjin, M. Rejab, Q. Halim, M. Merzuki, M. Darus, Experimental investigation of the tensile test using digital image correlation (DIC) method, Mater. Today: Proc. 27 (2020) 757–763.
[31] M. Quanjin, I.M. Sahat, M.R. Mat Rejab, S. Abu Hassan, B. Zhang, M.N. Merzuki, The energy-absorbing characteristics of filament wound hybrid carbon fiber-reinforced plastic/polylactic acid tubes with different infill pattern structures, J. Reinf. Plast. Compos. 38 (23–24) (2019) 1067–1088.
[32] A. D-21, Standard Test Method For Determination of External Loading Characteristics of Plastic Pipe By Parallel-Plate Loading, American Society for Testing and Materials West Conshohocken, 2021.
[33] G. Sun, Z. Wang, J. Hong, K. Song, Q. Li, Experimental investigation of the quasi-static axial crushing behavior of filament-wound CFRP and aluminum/CFRP hybrid tubes, Compos. Struct. 194 (2018) 208–225.
[34] Q. Ma, M. Rejab, A.P. Kumar, H. Fu, N.M. Kumar, J. Tang, Effect of infill pattern, density and material type of 3D printed cubic structure under quasi-static loading, Proc. Inst. Mech. Eng. Part C J. Mech. Eng. Sci. 235 (19) (2021) 4254–4272.
[35] D. ASTM, Standard test method for ignition loss of cured reinforced resins, in: ASTM, 2011.
[36] M. Quanjin, M. Rejab, M. Idris, S.A. Hassan, N.M. Kumar, Effect of winding angle on the quasi-static crushing behaviour of thin-walled carbon fibre-reinforced polymer tubes, Polym. Polym. Compos. 28 (7) (2020) 462–472.
[37] F. Eggers, J.H.S. Almeida Jr., C.B. Azevedo, S.C. Amico, Mechanical response of filament wound composite rings under tension and compression, Polym. Test. 78 (2019), 105951.
[38] S. Li, X. Guo, Q. Li, D. Ruan, G. Sun, On lateral compression of circular aluminum, CFRP and GFRP tubes, Compos. Struct. 232 (2020), 111534.